Vacuum 110 (2014) 121–126

Contents lists available at ScienceDirect

Vacuum

journal homepage: www.elsevier.com/locate/vacuum

Microstructure and hardness studies of electron beam welded Inconel 625 and stainless steel 304L

M. Shakil [a, b, *], M. Ahmad [b], N.H. Tariq [c], B.A. Hasan [c], J.I. Akhter [b], E. Ahmed [b], M. Mehmood [c], M.A. Choudhry [a], M. Iqbal [b]

[a] Department of Physics, The Islamia University of Bahawalpur, Bahawalpur 63100, Pakistan
[b] Physics Division, Pakistan Institute of Nuclear Science & Technology, P.O. Nilore, Islamabad, Pakistan
[c] DMME, Pakistan Institute of Engineering and Applied Sciences, P.O. Nilore, Islamabad, Pakistan

ARTICLE INFO

Article history:
Received 19 April 2014
Received in revised form
27 August 2014
Accepted 28 August 2014
Available online 16 September 2014

Keywords:
Inconel 625
SS 304L
Electron beam welding (EBW)
Fusion zone
Scanning electron microscopy (SEM)

ABSTRACT

In this study, electron beam welding of dissimilar Inconel 625 and SS 304L alloys was successfully performed by employing optimized electron beam welding parameters. The welded joint was characterized using SEM/EDS, XRD and micro-hardness tester. The welded joint was found homogeneous, well bonded and defect free. Two types of microstructure i.e. columnar dendritic and cellular dendritic were observed in the fusion zone. The development of different microstructures in the fusion zone was attributed to the localized cooling effects during solidification. Few micro-cracks along with dendrites splitting were observed in the vicinity of end crater that was mainly due to the segregation of S element. A significant variation of Ni and Fe was observed across Inconel/FZ and FZ/SS interfaces due to their fast diffusion in the melt pool. Micro-hardness measurements across Inconel/FZ and FZ/SS interfaces showed an increasing trend in the FZ from SS 304L towards Inconel base alloy.

1. Introduction

Welding of dissimilar materials has been the subject of interest of many researchers due to their high demand for various industrial applications. Dissimilar materials are welded in order to increase flexibility in design and application. However, this practice may often create problems that severely affect the performance during service. The welding of two dissimilar alloys with different thermal expansion coefficient, melting temperature is a complicated task [1,2]. Inconel 625 is a Nickel base superalloy strengthened by a solid solution of molybdenum and niobium in its nickel–chromium matrix. It has wides pread applications in aerospace, marine, chemical, petrochemical industries due to its superior physical and chemical properties i.e high strength, corrosion and creep resistance at elevated temperatures. The alloy has also some applications in nuclear power plant reactor-core and control rod components of pressurized water reactor. It is also being used as a heat exchanger tube in ammonia cracker plants of heavy water production [3,4]. Stainless steel 304L is a less expensive structural material that found applications within general corrosive environments, reprocessing plants and nuclear power plant components. During welding process its lower carbon content reduces the precipitation of carbide in the fusion zone. Nickel-based alloys and stainless steel (SS) have extensive applications in the manufacturing of components used in pressurized water reactors and boiling water reactors in nuclear power plants [5]. To fabricate these parts traditional welding techniques such as shield metal arc welding (SMAW), gas tungsten arc welding (GTAW) and gas metal arc welding (GMAW) are normally used. However, in conventional welding techniques large numbers of welding passes are required to join thick parts for achieving sufficient strength in the weld metal. The increased number of passes produces greater thermal cycling effect resulting in the formation of carbide. The high heat input and large heat affected zone (HAZ) in afore-mentioned conventional welding techniques result in reduced corrosion resistance and mechanical properties of the welded joint [6–14].

Electron beam welding (EBW) is a high energy density beam welding that is capable of welding thick parts in a single pass. EBW has a number of significant benefits over other welding techniques i.e lower total heat input, smaller HAZ, a high depth to width ratio and low residual stress in the weld. EBW can produce deep weld as

* Corresponding author. Department of Physics, The Islamia University of Bahawalpur, Bahawalpur 63100, Pakistan. Tel.: +92 321 6828243.
E-mail addresses: shakil101@yahoo.com, m.shakil@iub.edu.pk, shakil101iub@hotmail.com (M. Shakil).

http://dx.doi.org/10.1016/j.vacuum.2014.08.016
0042-207X/

Table 1
Nominal composition (wt%) of welded alloys.

Alloys	Ni	Cr	Mn	Si	Fe	Mo	Nb	Al	Ti	S
Inconel 625	Bal.	22.76	0.20	0.37	4.18	7.96	2.86	0.36	0.39	0.28
SS 304L	9.72	19.32	1.78	0.47	Bal.	–	–	–	–	0.23

compared to other welding processes. These advantages thus provide defect free welded joint as well as reduce the welding stresses in the fusion zone (FZ). In addition, the high efficiency of EBW reduces the welding time, improves the safety and reliability of welded parts [15–20]. In the present work, EBW has been successfully employed to join Inconel 625 with SS 304L to achieve defect free dissimilar welded part. It is anticipated that the results of this work would be very useful for advanced industrial applications of dissimilar Inconel 625/SS 304L welded joints.

2. Experimental

The samples of Inconel 625 and SS 304L with dimensions 10 mm × 10 mm × 3 mm were cut from the sheets using slow speed cutter. Nominal composition of as received Inconel 625 and SS 304L is provided in Table 1. The samples were ultrasonically cleaned and polished on a lapping machine using diamond paste down to 0.25 μm. Joining sides of both metals were also polished up to the same level. The samples were placed together in a locally designed special die to hold them in such a way that they could not separate from each other during the course of welding. Electron beam welding was performed in a continuous mode, normal to the sample surface by employing various combinations of welding parameters, the beam current and welding speed, under vacuum and optimized values were selected. The welding parameters used are provided in Table 2. A schematic illustration of the design of the weldment is shown in Fig. 1.The weldment was placed on a thick copper sheet (large heat sink) to ensure that the heat source of electron beam is uniformly distributed along the Inconel 625 and SS 304L plate. The experiment was performed using TECHMETA, France EBW machine having maximum voltage 60 kV and maximum current 50 mA. After welding, the welded sample was again polished and etched chemically. The microstructure and elemental distribution was investigated by Scanning Electron Microscope equipped with Energy Dispersive Spectrometer (EDS). In order to determine the phases in the weld zone X-ray diffraction (XRD) scan was performed. Finally, microhardness was measured across the weld interface using Vickers hardness tester by using a load of 300 g at room temperature.

3. Results and discussion

In order to achieve a crack and defect free weld interface, the beam current (I) and welding speed (v) were optimized after conducting series of preliminary experiments with the aim to reduce welding residual stresses at weld interfaces. Welding residual stresses could be reduced by controlling cooling rate (R) of the fusion zone which has following relationship with beam current and welding speed [21];

$$R \propto (v/I)^2$$

According to the above equation, a moderate cooling rate can be achieved through the balance between welding speed and beam current. Based on the observed microstructure, the operating parameters were optimized by a systematic increase in the beam current from 20 to 30 mA at different welding speeds ranging from 400 to 700 mms^{-1}. Fig. 2 shows the low magnification SEM micrographs of the welded samples under different welding parameters. A sound and defect free joint was achieved at beam current of 25 mA and 600 mms^{-1} welding speed as shown in Fig. 2(c).

Table 2
Electron beam welding parameters.

Parameters	Values
Voltage	30 kV
Current	20, 25, 30 mA,
Power	600, 750, 900 W
Vacuum	1.3×10^{-6} mbar
Welding speed	400, 500, 600, 700 mm/min
Welding Pass	1
Welding mode	Continuous

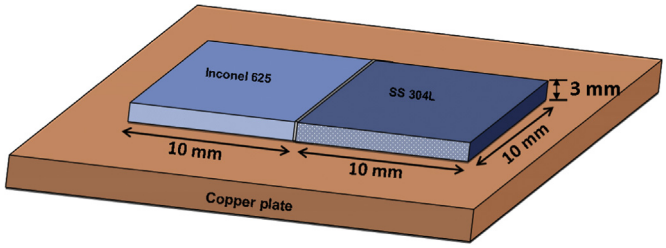

Fig. 1. A schematic illustration of the design of the weldment with a large heat sink of copper.

3.1. Microstructure

Fig. 3 shows low magnification SEM micrograph of EB welded Inconel 625 and SS 304L. Interfaces of FZ with both of the alloys are clearly seen. It was observed that FZ was gradually widened towards its end (bottom of Fig. 3). This phenomenon was mainly due to high heat buildup at the end of FZ [22]. In order to further investigate the bonded region, Inconel/FZ and FZ/SS interfaces (marked by regions 1 and 2 respectively in Fig. 3) were further magnified as shown in Figs. 4 and 5. It is quite evident from Figs. 4 and 5 that the interfaces are quite homogeneous, well bonded and defect free. Only few micro cracks along with some dendrite splitting were observed in the vicinity of end crater (marked by region-4 in Fig. 3), otherwise, the entire weld was crack free. The formation of these micro cracks and separated grain boundaries at the end of FZ is either due to the solidification shrinkage during solidification and/or the segregation of minor alloying elements/impurities [23,24]. Kou et al. reported thermal shrinkage liable for these cracks/defects that exist in intergranular and dendritic morphology in the FZ during the end stage of solidification [24] (Fig. 7). These micro cracks were also reported by Patterson et al. during the welding of austenitic stainless steels and nickel alloys due the segregation of S, P, Ti and Nb elements [25]. However, in the present scenario, segregation of S was only witnessed around cracks as evident by EDS point analysis shown in Fig. 7. The chemical composition of various regions of the weld is summarized in Table 3. The composition determined in the cracks showed an increased amount of Sulphur as compared to the base alloys composition.

Fig. 8 shows the high magnification SEM micrograph of FZ area (marked by region-3 in Fig. 3) showing dendritic microstructure composed of two types namely, columnar dendrites and cellular dendrites. This microstructure is attributed to the different thermophysical properties of Inconel 625 & SS 304L including thermal conductivity and specific heat which vary with temperature. For instance the thermal conductivities of Inconel 625 & SS 304L at

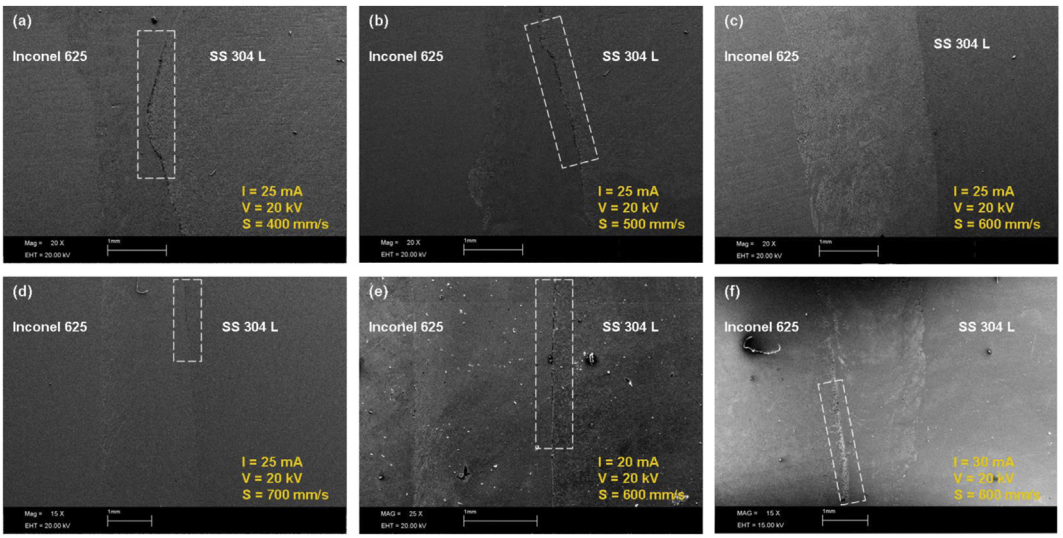

Fig. 2. Low magnification SEM micrographs of Inconel 625/SS 304L welds obtained at different welding parameters. The regions marked by rectangles show weld defects.

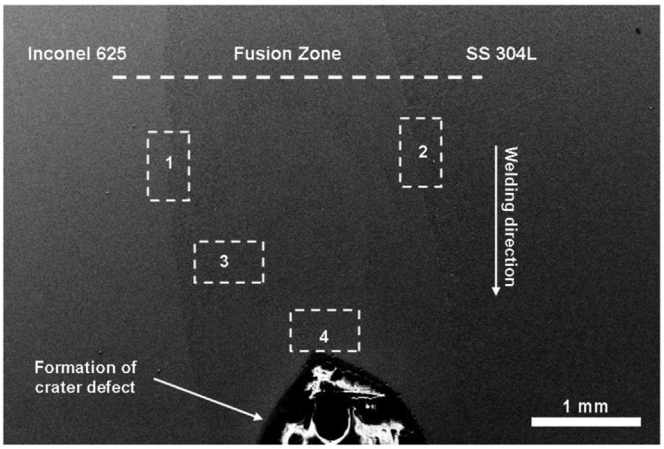

Fig. 3. SEM micrograph of Inconel 625/SS 304L weld at optimized welding conditions.

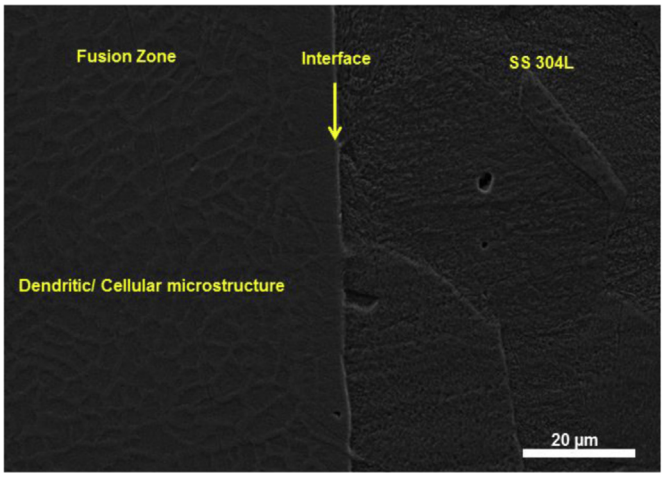

Fig. 5. SEM micrograph showing interface between Fusion zone and SS.

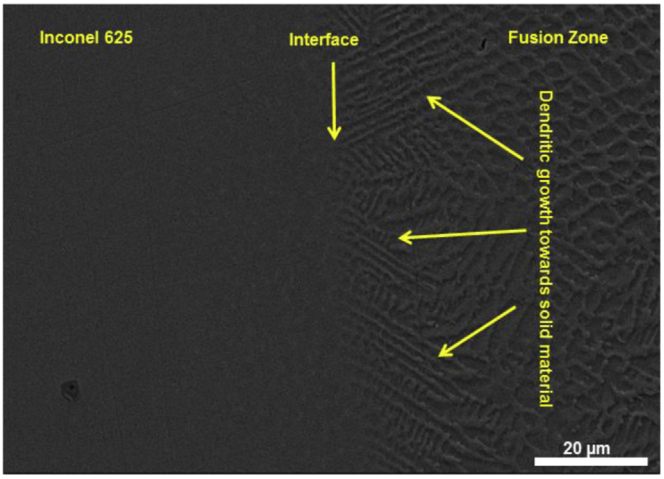

Fig. 4. SEM micrograph showing the interface between Inconel 625 and FZ.

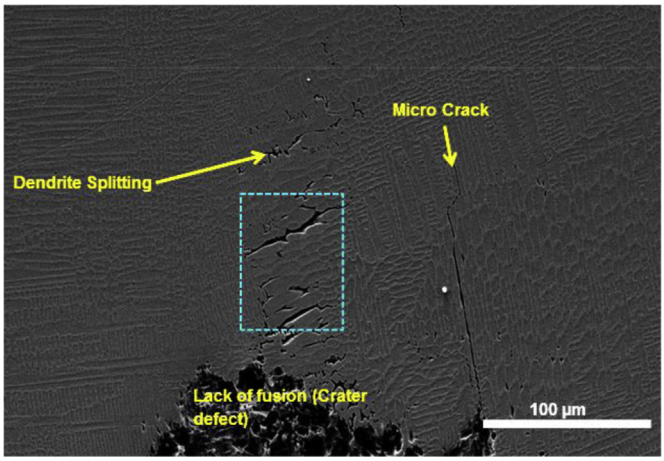

Fig. 6. SEM micrograph showing the presence of cracks at the bottom of FZ.

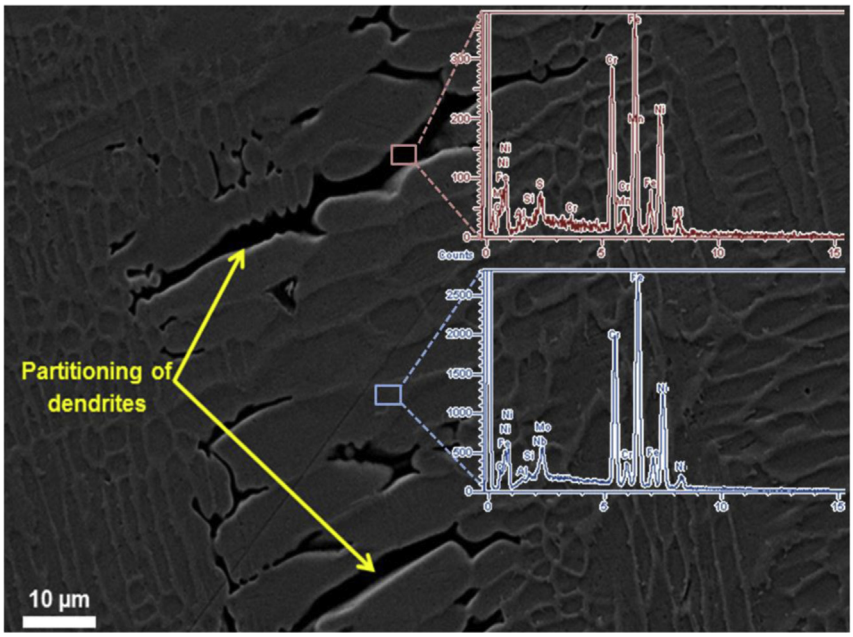

Fig. 7. High magnification SEM micrograph of the region marked by a rectangle in Fig. 6.

100 °C are 11.4 and 16.3 Wm^{-1} K^{-1} that changes to 17.5 and 21.4 Wm^{-1} K^{-1} at 500 °C. It is obvious that in the weldment, the Inconel 625 side would have a significantly steeper temperature gradient as compared to SS 304L starting from the center line of the FZ to the end to the specimen at either side. S. Kou et al. [1] indicated that solidification structure of welded products is determined by the degree of constitutional supercooling (i.e. the ratio of the temperature gradient (G) to the growth rate (R), G/R) during solidification. Furthermore, the product $G \times R$ is equivalent to the cooling rate. Larger thermal gradients during EBW favor the formation of complex microstructures due to the non-equilibrium conditions during the rapid solidification of FZ. The thermal gradients are larger for high energy density welding processes such as EBW and laser beam welding. It is lowest along the weld center line and found maximum at the fusion line when moving outward from center line along the solidification front [26]. In Fig. 8, the area consisted of columnar dendrites is very small and located near the edge of the FZ towards the Ni-alloy solid surface. The possible reason for the formation of columnar dendrites may be the much lower thermal conductivity of Inconel 625 in comparison to SS 304L which results in small heat dissipation in this area. As a result, slightly higher values of G/R, associated with lower constitutional supercooling, were achieved. Similar dendritic microstructure was observed by other researchers in Ni-base single crystal alloy during the EB treatment [20]. The dendritic growth and latent heat dissipation in FZ are anti-parallel in the case of columnar dendritic structure, whereas, it is parallel in cellular structure [20]. The average composition taken in the core of dendrites and at inter dendritic area is listed in Table 3. The dendritic core was found to be enriched in Ni, Mo, and Nb as compared to the other areas around the core. On the other hand uniform equiaxed cellular structure (not shown) was observed in the central region of the FZ. The occurrence of equiaxed structure in the central area is attributed to the uniform and symmetric cooling as compared to the edges of the FZ. The equiaxed cellular structure is highly depending upon the alloy composition, turbulence and thermal gradients at S/L interface. As revealed by EDS discussed later (Table 2), the chemical composition of FZ was based on a mixture of both Inconel 625 and SS 304L. So, FZ may have wide spread between Liquidus and Solidus temperatures which often favors formation of he equiaxed cellular structure. Secondly, the equiaxed cellular structure might be formed due to the low thermal gradients at S/L interface towards SS

Table 3
Quantitative analysis of different regions in the FZ.

	Ni	Cr	Mo	Nb	Fe	Si	Al	S	Mn
Inconel 625(base metal)	59.97	22.76	7.96	2.86	4.18	0.37	0.36	0.28	0.20
SS 304L (base metal)	9.72	19.32	–	–	68.48	0.47	–	0.23	1.78
Fusion Zone	27.83	22.55	2.50	1.03	43.98	0.88	0.49	–	0.89
Cracks boundary	31.01	23.53	–	–	40.00	–	–	2.57	–
Inside the cracks	28.61	26.17	–	–	41.62	1.19	–	1.89	–
Cellular boundaries	28.26	22.70	2.88	1.13	42.26	0.98	–	–	–
Inside the cells	27.59	21.82	2.15	–	46.35	–	–	–	–
Dendrite cores	36.66	22.69	3.79	2.00	32.73	–	–	–	–
Inter dendritic area	29.94	22.46	2.21	–	43.37	–	–	–	–

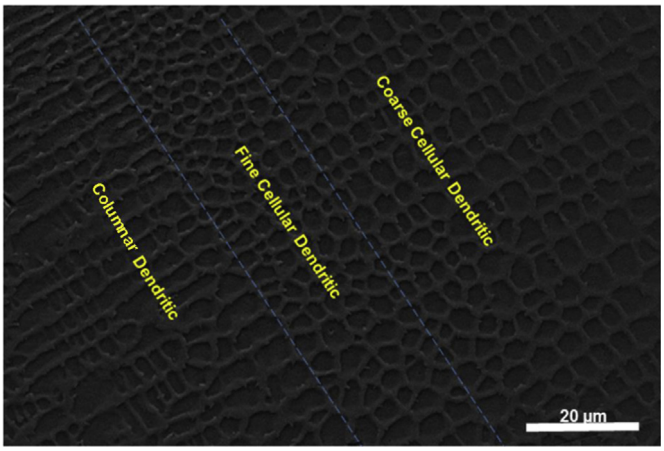

Fig. 8. SEM micrograph of an FZ region (marked by region-3 in Fig. 3) showing columnar and cellular dendrites.

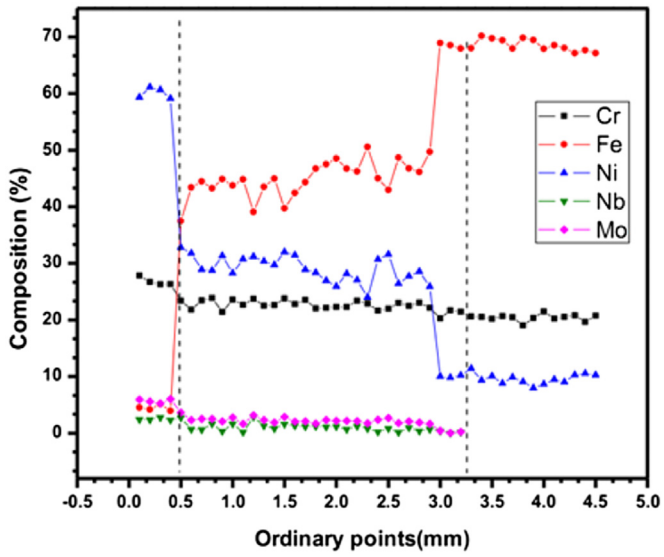

Fig. 9. EDX point analysis across FZ/Inconel and FZ/SS interfaces.

304L side. In other words, much lower G/R ratio was achieved at central region.

It is again clear from Table 3 that the dendritic cells boundaries are enriched in Mo and Nb as compared to the inner areas of cellular structures. Since Mo and Nb have large radii in comparison to the other elements in the melt pool, they cause segregation during the terminal solidification. It has been reported in the literature that in Nb-bearing superalloys, the terminal solidification is different due to the presence of Nb element which is a strong segregant controlling terminal solidification reaction [27].

In order to determine compositional variation across Inconel/FZ interface, FZ and FZ/SS interface, EDS microanalysis (Fig. 9) was performed along the white dash line indicated in Fig 3. A significant variation of Ni and Fe was observed across Inconel/FZ and FZ/SS interfaces. The large variation of Ni and Fe in FZ was mainly due to their fast diffusion in the melt pool, since Ni and Fe have small atomic radii in comparison to other weld metal constituent elements.

3.2. X-ray diffraction

XRD pattern of Inconel 625, SS 304L, and welded zone is shown in Fig. 10. It was also revealed that the XRD pattern of Inconel alloy was much similar with that of FZ. This indicates that both FZ and Inconel alloy have almost same crystal structure. However, EDS analysis (Table 2) revealed that the chemical composition of FZ was based on a mixture of Inconel 625 and SS 304L. It can be clearly seen from Fig. 10 that the base Inconel 625 alloy as well as FZ show the presence of Ni (fcc) solid solution with lattice parameter of 360.58 pm and 360.60 pm respectively. More or less same γ-Ni matrix lattice parameter of base Inconel 625 alloy as well as FZ indicates that no intermetallic phases like γ', γ'' or δ were precipitated out in the matrix. Since the cooling rate during EBW is very high, most of the strengthening elements like Nb and Mo remained in the solid solution of γ-Ni matrix and formed no precipitates. It was also observed that XRD peaks intensity of FZ was decreased and slightly shifted towards the lower angles which might be attributed to the residual stresses induced by fast cooling of FZ [20] and large variation of Ni and Fe content in the FZ (Table 3, Fig. 9).

3.3. Micro-hardness

The micro-hardness measurements were made by using Vickers hardness tester. Fig. 11 shows the difference in hardness values between the Inconel 625, FZ, and SS 304L. Inconel 625 is a solution strengthened Ni-based superalloy with higher hardness values as compared to the SS 304L. The approximate length of FZ was found to be 2.4 mm. The hardness measured in the FZ showed overall an increasing trend moving from SS 304L side towards the Inconel alloy.

The hardness in the weld increased from 150 to 225 HVN. This might be caused by alterations in the structure across the weld cross-section. However, within the FZ the hardness values were scattered that may be attributed to the convection effects in the weld metal as well as due to the variation of supersaturation of Nb and Mo strengthening elements in the γ-matrix.

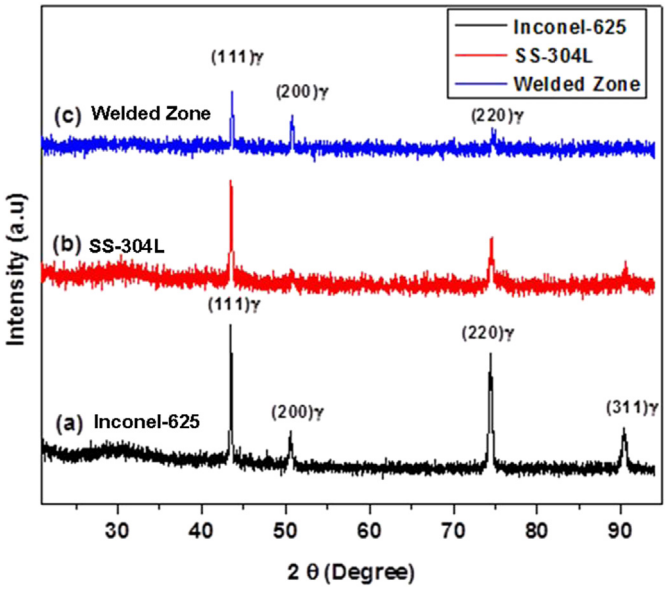

Fig. 10. XRD pattern of (a) Inconel 625 (b) SS 304L and (c) Fusion zone.

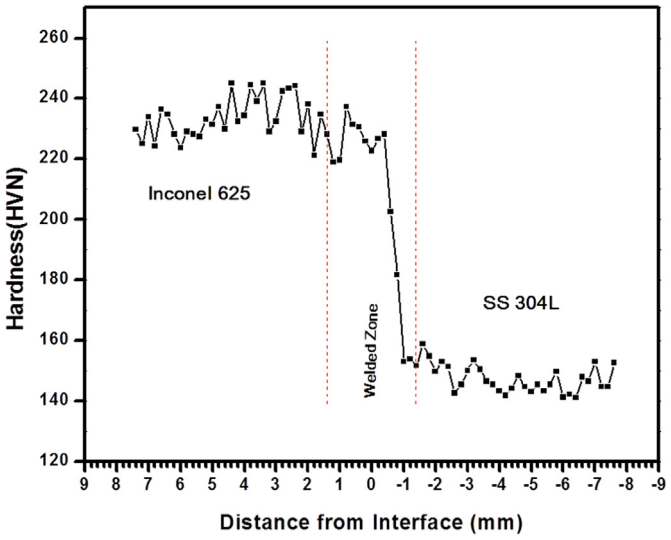

Fig. 11. Microhardness profile across the FZ.

4. Conclusions

Electron beam welding of dissimilar Inconel 625 and SS 304L alloys was achieved by employing optimized electron beam welding parameters. The welded joint was found homogeneous, well bonded and defect free. Different types of microstructures were evolved in the fusion zone due to the localized cooling effects during solidification. Few micro-cracks along with dendrites splitting were observed in the vicinity of end crater which was mainly due to the segregation of S element. Micro-hardness measurements across Inconel/FZ and FZ/SS interfaces showed an increasing trend in the FZ from SS 304L towards Inconel base alloy.

Acknowledgments

The authors gratefully acknowledged the financial support provided by the Higher Education Commission (HEC) Pakistan for this work.

References

[1] Kou S. Welding metallurgy. 2nd ed. New York: Wiley-Inter Science; 2003.
[2] Richard Avery E. Pay attention to dissimilar-metal welds. Avery Consulting Associates Inc; 2003. p. 1–6.
[3] Sims CT, Stollof NS, Hagel WC. Superalloys. 2nd ed. New York: Wiley-Inter Science; 1987.
[4] Shankar V, Rao KBS, Mannan SL. J Nucl Mater 2001;288:222–32.
[5] Ishihiara T. Weld J 1989;68:209–16.
[6] Stiller K, Nilsson JO, Norring K. Metall Mater Trans A 1996;27A:327–41.
[7] Kuo TY, Lee HT. Mater Sci Eng A 2002;338:202–12.
[8] Lee HT, Jeng SL. Sci Technol Weld Join 2001;6:225–34.
[9] Lee HT, Kuo T. Sci Technol Weld Join 1999;4:94–103.
[10] Horn RM, Gordon GM, Ford FP, Cowan RL. Nucl Eng Des 1997;9:313–25.
[11] Jeng SL, Lee HT, Rehbach WP, Kuo TY, Mayer JP. Mater Sci Eng A 2005;397:229–38.
[12] Lee HT, Jeng SL, Yen CH, Kuo TY. J Nucl Mater 2004;335:59–69.
[13] Lee HT, Jeng SL, Kuo TY. Metall Mater Trans A 2003;34:1097–2005.
[14] Kuo TY, Lee HT, Tu CC. Sci Technol Weld Join 2003;8:39–48.
[15] Stone HJ, Roberts SM, Reed RC. Metall Mater Trans A 2000;31A:2261–73.
[16] Sun Z, Karppi R. J Mater Process Technol 1996;59:257–67.
[17] Lim YS, Kim JS, Kwon HS. Mater Sci Eng A 2000;279:192–200.
[18] Tariq NH, Shakil M, Hasan BA, Akhter JI, Haq MA, Awan NA. Vacuum 2014;101:98–101.
[19] Ahmad M, Ali G, Ahmed E, Haq MA, Akhter JI. Appl Surf Sci 2011;257:7405–10.
[20] Ahmad M, Ali G, Akhter JI, Akhtar M, Chaudhry MA. J Alloy Compd 2008;461:102–5.
[21] Yokoyamaa Y, Abeb N, Fukaura K, Shinohara T, Inoue A. Mater Sci Eng A 2004;375–377:422–6.
[22] Schultz H. Electron beam welding. Woodhead Pub; 1993. Shultz, 1993.
[23] Ahmad M, Akhter JI, Shahzad M, Akhtar M. J Alloy Compd 2008;1–2:131–4.
[24] Kou S. JOM 2003;55:37–42.
[25] Patterson RA, Milewisky JO. Weld Res Suppl 1985;8:227s–31s.
[26] David SA, Vitek JM. Int Mater Rev 1989;34:213–45.
[27] Dupont JN, Banovic S, Marder A. Weld J 2003;82:125s–35s.